

FEATURE ARTICLE

Computational Studies of the Photophysics of Hydrogen-Bonded Molecular Systems

Andrzej L. Sobolewski*,† and Wolfgang Domcke‡

Institute of Physics, Polish Academy of Sciences, PL-02668 Warsaw, Poland, and Department of Chemistry, Technical University of Munich, D-85747 Garching, Germany

Received: July 24, 2007; In Final Form: August 20, 2007

The role of electron- and proton-transfer processes in the photophysics of hydrogen-bonded molecular systems has been investigated with ab initio electronic-structure calculations. Adopting indole, pyridine, and ammonia as molecular building blocks, we discuss generic mechanisms of the photophysics of isolated aromatic chromophores (indole), complexes of π systems with solvent molecules (indole–ammonia, pyridine–ammonia), hydrogen-bonded aromatic pairs (indole–pyridine), and intramolecularly hydrogen-bonded π systems (7-(2'-pyridyl)indole). The reaction mechanisms are discussed in terms of excited-state minimum-energy paths, conical intersections, and the properties of frontier orbitals. A common feature of the photochemistry of the various systems is the electron-driven proton-transfer (EDPT) mechanism: highly polar charge-transfer states of ${}^1\pi\pi^*$, ${}^1n\pi^*$, or ${}^1\pi\sigma^*$ character drive the proton transfer, which leads, in most cases, to a conical intersection of the S_1 and S_0 surfaces and thus ultrafast internal conversion. In intramolecularly hydrogen-bonded aromatic systems, out-of-plane torsion is additionally needed for barrierless access to the S_1 – S_0 conical intersection. The EDPT process plays an essential role in diverse photophysical phenomena, such as fluorescence quenching in protic solvents, the function of organic photostabilizers, and the photostability of biological molecules.

1. Introduction

Hydrogen bonds are of universal importance in chemistry and biochemistry. Examples are the structure and dynamics of liquids and molecular crystals (such as water and ice), solvation in protic solvents, molecular recognition (e.g., in DNA) and the catalytic reactivity of enzymes. The properties of hydrogen bonds in the electronic ground state have been investigated for decades with powerful experimental methods, such as infrared (IR) and Raman vibrational spectroscopy and neutron scattering, and are thus quite well understood.¹ Because hydrogen bonding is essentially an electrostatic effect, it can quite accurately be described by cost-effective ab initio methods such as restricted Hartree–Fock (RHF), second-order Møller–Plesset perturbation

theory (MP2) or density functional theory (DFT). These computational methods can nowadays be applied to rather large molecular systems, including those of biological interest, see, e.g., refs 2 and 3.

Much less is known, in general, about the properties of hydrogen bonds in excited electronic states and their role in photochemical processes. A notable exception are aromatic systems with an intramolecular hydrogen bond that exhibit the phenomenon of excited-state intramolecular proton transfer (ESIPT).^{4–6} These systems are of considerable applied interest as photostabilizers and sunscreens for the protection of organic polymers and biological tissues.^{7,8} The questions of the time scale of the excited-state proton transfer and the presence or absence of a barrier have been a matter of dispute for a long time.^{4–6} Another widely studied phenomenon involving excited-state dynamics of hydrogen bonds is fluorescence quenching in intermolecularly hydrogen-bonded aromatic chromophores.^{9–14}

* Corresponding author. E-mail: sobola@ifpan.edu.pl.

† Polish Academy of Sciences.

‡ Technical University of Munich.



Andrzej L. Sobolewski received his MSc in Physics from Warsaw University, Poland, in 1977 and was employed as an assistant at the Institute of Physics of the Polish Academy of Sciences (IPPAS) where he received his Ph.D. in 1981. He worked for two years as a postdoctoral Humboldt fellow at the Technical University of Munich. Having received the Habilitation degree in 1989 in the IPPAS, he obtained professor position there. His research interests include, among others, investigation of elementary photochemical processes in biomolecular systems, e.g., excited-state proton and electron transfer, and pathways of radiationless energy relaxation.

A mechanistic explanation of the highly effective deactivation of fluorescent states in terms of curve-crossing dynamics involving a dark charge-transfer (CT) state has been proposed by Mataga.¹² This model remained speculative, however, because it could not be supported by accurate ab initio electronic-structure calculations at that time. A third active area of research is the real-time investigation of optically triggered neutralization reactions of acid–base pairs in water.^{15,16}

One reason for our rather limited knowledge of excited-state hydrogen-bond dynamics is the extremely short time scale of these processes, which often may be beyond the limit of present-day time resolution of pump–probe experiments in the ultraviolet (UV) (about 10 fs). Another reason is the difficulty of performing accurate ab initio electronic-structure calculations for excited electronic states of polyatomic molecules. Excited electronic states are open-shell, generally multiconfigurational, and often subject to intricate valence–Rydberg mixing effects. Apart from the complexities of the electronic structure, chemically interesting excited-state dynamics involves large-amplitude nuclear motion such as fragmentation or chemical rearrangement. The identification of the chemically relevant nuclear degrees of freedom, in particular minimum-energy reaction paths, requires the exploration of truly high-dimensional potential-energy (PE) surfaces over extended regions. The necessary tools, in particular multiconfiguration (MC) self-consistent-field (SCF) methods, multireference (MR) perturbation-theory methods, and analytic energy gradients for efficient geometry optimization have become available only relatively recently.¹⁷

In this Feature Article, we provide an overview, at a largely qualitative level, of the insights that can be obtained into the photophysics and photochemistry of intramolecular and intermolecular hydrogen bonds by the application of state-of-the-art electronic-structure calculations. For this purpose, we have selected the molecular building blocks shown in Figure 1. Indole serves as the representative of proton-donating aromatic chromophores (often referred to as photoacids). Pyridine represents an aromatic proton acceptor (often called photobase). Ammonia is chosen as an example of an amphoteric saturated solvent molecule. From these three molecular bricks, we have constructed the four hydrogen-bonded model systems shown in Figure 2. The indole–ammonia complex (Figure 2a) has been chosen for the investigation of the mechanistic aspects of the



Wolfgang Domcke received his diploma and Ph.D. degrees in Physics from the Technical University of Munich (TUM), Germany, in 1973 and 1975, respectively. He then became a research associate in the Physics department of the University of Freiburg. Having received the Habilitation degree in 1979, he became associate professor of Theoretical Chemistry at the University of Heidelberg and later at the TUM. In 1996, he became full professor at the University of Düsseldorf. In 1999, he returned to the TUM, where he currently is professor of Theoretical Chemistry. His research interests comprise, among others, the application of electronic-structure theory for the calculation of excited-state potential-energy surfaces, the theoretical description of nonadiabatic dynamics in photochemistry, and the theory of nonlinear time-resolved electronic spectroscopy of polyatomic molecules.

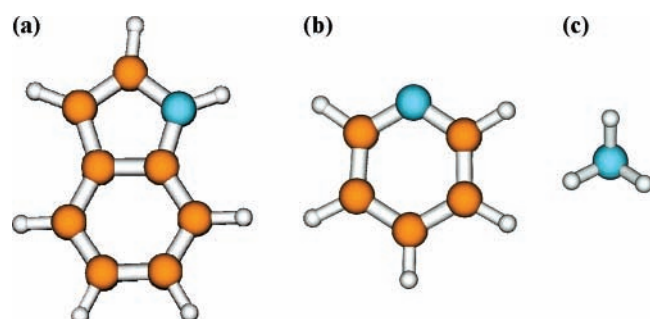


Figure 1. Molecular bricks used for the construction of hydrogen-bonded systems: (a) indole, proton donor; (b) pyridine, proton acceptor; (c) ammonia, amphoteric solvent molecule.

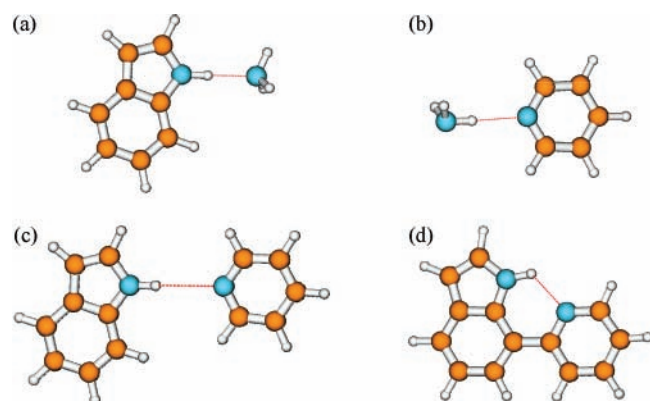


Figure 2. Hydrogen-bonded complexes considered in this work: (a) indole–ammonia complex; (b) pyridine–ammonia complex; (c) indole–pyridine complex; (d) 7-(2'-pyridyl)indole.

hydrogen transfer from photoacids to hydrogen-accepting solvents. The pyridine–ammonia complex (Figure 2b) serves as a model for the investigation of the photophysics of a photobase in a hydrogen-donating solvent environment. The indole–pyridine hydrogen-bonded complex (Figure 2c) will provide insight into the mechanisms of fluorescence quenching via hydrogen bonds. Figure 2d, finally, shows 7-(2'-pyridyl)-

indole as an example of an intramolecularly hydrogen-bonded π system, for which the mechanisms of the ESIPT process and the function of organic photostabilizers can be investigated.

2. Computational Methods

The ground-state equilibrium geometries of the molecular systems considered in this work have been determined with the MP2 method. Excitation energies and response properties have been calculated with the CC2 method,^{18,19} which is a simplified and computationally efficient version of the coupled-cluster method with singles and doubles (CCSD). The equilibrium geometries of the lowest excited singlet states have been determined at the CC2 level, making use of the recently implemented CC2 analytic gradients.²⁰ Dunning's correlation-consistent split-valence double- ζ basis set with polarization functions on all atoms (cc-pVDZ)²¹ was generally employed in these calculations, with the exception of the $^1\pi\sigma^*$ state in indole and in the indole–ammonia complex, where this basis set was augmented by diffuse functions at the nitrogen(s), which were taken from the aug-cc-pVDZ basis set. The vertical excitation energies and spectroscopic properties were calculated at the CC2/aug-cc-pVDZ level. For the smaller systems (indole, indole–ammonia, and pyridine–ammonia), these properties were additionally calculated with the aug-cc-pVTZ basis set (see Supporting Information (SI)).

All MP2 and CC2 calculations were carried out with the TURBOMOLE program package,²² making use of the resolution-of-the-identity (RI) approximation for the evaluation of the electron-repulsion integrals.²³

The minimum-energy reaction paths of the photophysically relevant reactions in the ground state and in the lowest excited singlet states have been determined with the MP2 and CC2 methods, respectively. For a suitably chosen driving coordinate, all other nuclear degrees of freedom have been optimized for a given value of the driving coordinate, which is the internal coordinate resembling most closely the desired reaction coordinate. To allow cost-effective explorations of the high-dimensional excited-state potential-energy functions, the standard split-valence double- ζ basis set with polarization functions on heavy atoms (def-SV(P)) of TURBOMOLE has been employed in these reaction-path calculations. The single-point energy calculations along the reaction path were performed with the CC2/cc-pVDZ method. For indole and the indole–ammonia complex, the aug-cc-pVDZ functions on nitrogen(s) were used in both sets of calculations.

3. Photoinduced Hydrogen Detachment from Aromatic Chromophores: Indole

As the first example, we consider the photoinduced hydrogen-abstraction process in bare indole. The understanding of the mechanisms of this comparatively simple photochemical process will be helpful for the discussion of photoinduced hydrogen-transfer processes in the following sections.

Several years ago, we pointed out that optically dark excited states of $^1\pi\sigma^*$ character play an essential role in the photochemistry of aromatic molecules with acidic groups, such as pyrrole, indole, or phenol.^{24–26} The energies of these $^1\pi\sigma^*$ states as a function of OH or NH bond lengths are generically dissociative and cross the PE function(s) of the $^1\pi\pi^*$ excited state(s) as well as the PE profile of the electronic ground state. These PE crossings, which are symmetry-allowed in the planar systems (because S_0 and $^1\pi\pi^*$ states transform as A' , and $^1\pi\sigma^*$ states transform as A''), become conical intersections^{27–29} when out-of-plane modes are taken into account. These conical

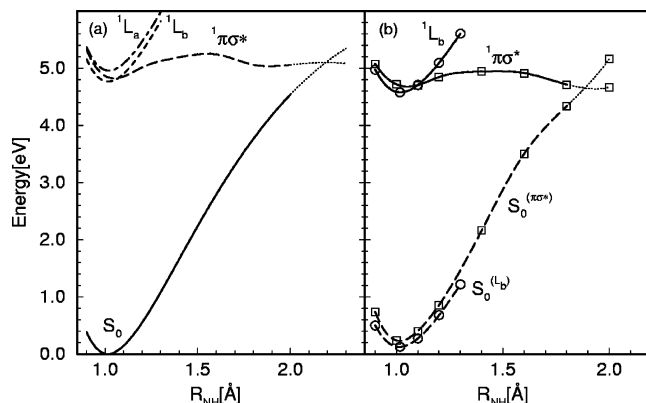


Figure 3. Potential-energy profiles of the ground state and the lowest excited states of indole as a function of the proton-detachment (NH stretching) coordinate: (a) rigid dissociation; (b) energy profiles along the minimum-energy path in the excited states (solid lines). Dashed lines in (b) represent the energy of the ground state calculated at the geometry of the respective excited state (designated as $S_0^{(\pi\sigma^*)}$ and $S_0^{(L_b)}$, respectively). Dotted lines indicate interpolations through regions where the CC2 calculations cannot be converged or are not considered to be reliable.

intersections can provide the pathway for efficient radiationless decay to the electronic ground state as well as hydrogen detachment.^{30,31}

The photoinduced hydrogen-detachment process is nowadays well understood in pyrrole and phenol. Several groups have detected the fast hydrogen atoms that result from the direct excited-state dissociation of pyrrole and phenol.^{32–37} The high-resolution photofragment translational spectra obtained by Ashfold and collaborators have revealed an unexpected mode-specificity of the photodissociation process: only a small subset of the available density of vibrational states is excited in the pyrrolyl or phenoxy radicals, confirming that very few vibrational degrees of freedom are actively involved in the dissociation process.^{34,37}

The PE surfaces of the relevant electronic states and their conical intersections have been characterized by ab initio calculations, taking the hydrogen-abstraction coordinate and the dominant coupling modes at the conical intersections into account.^{30,31,38} The dynamics at the conical intersections has been visualized by two-dimensional or three-dimensional quantum wave packet dynamics calculations.^{30,31,38}

The existence of the photoinduced hydrogen-detachment process in indole has been confirmed by Lin et al.³⁹ and Nix et al.⁴⁰ The corresponding PE profiles, calculated at the CC2 level with the aug-cc-pVDZ basis set, are shown in Figure 3. Here, as well as in the following, we show two types of PE functions. Figure 3a gives the PEs for rigid abstraction of the hydrogen atom of the NH group, starting from the equilibrium geometry of the electronic ground state. All internal coordinates, except the NH distance, have been kept fixed in this calculation. Figure 3b, on the other hand, shows the PE profiles calculated along the C_s -constrained minimum-energy path for hydrogen detachment. In this case, the energy has been optimized with respect to all in-plane internal coordinates for either the 1L_b ($\pi\pi^*$) state or the $^1\pi\sigma^*$ state. The energy of the S_0 state has been calculated at the geometries optimized for the $^1\pi\sigma^*$ state (dashed line with squares) or the 1L_b state (dashed line with circles). All the curve crossings in Figure 3a and the crossing of the $^1\pi\sigma^*$ and $S_0^{(\pi\sigma^*)}$ curves in Figure 3b are true crossings (conical intersections), because these energies have been calculated at the same geometries. The crossings of the 1L_b and $^1\pi\sigma^*$ curves in Figure

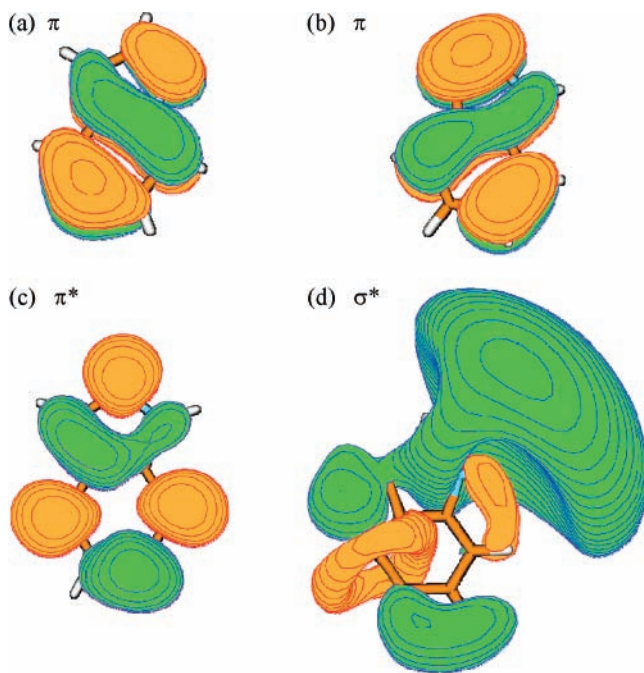


Figure 4. The two highest occupied π orbitals (a, b) the lowest unoccupied π^* orbital (c), and the σ^* orbital (d) of indole, determined at the equilibrium geometry of the electronic ground state. The colors encode the sign of the wave function.

3b, on the other hand, are apparent crossings, because these PE functions have been calculated for different geometries.

The comparison of Figure 3a,b reveals that the ${}^1\pi\sigma^*$ -driven dissociation of the NH group of indole is very weakly coupled with other degrees of freedom: the PE profiles for rigid NH dissociation and dissociation along the minimum-energy path are essentially identical. This result is in full accord with the experimental observation that very few vibrations of the indolyl radical become excited in the photoinduced hydrogen-detachment process.⁴⁰ Both the computational results as well as experimental observations provide strong evidence that the photoinduced hydrogen-detachment process in indole can be described by low-dimensional wave packet calculations in analogy to pyrrole and phenol.^{30,31}

The CC2/aug-cc-pVDZ PE functions of Figure 3 indicate that the vertical excitation energy of the ${}^1\pi\sigma^*$ state is nearly degenerate with the closely spaced 1L_b and 1L_a states. Previous results obtained with the CASPT2 method and a basis set with less diffuse functions had predicted a larger ${}^1\pi\pi^*-{}^1\pi\sigma^*$ vertical energy gap.²⁴ This difference is partly due to the fact that CC2 overestimates the excitation energies of ${}^1\pi\pi^*$ states, and CASPT2 tends to underestimate the ${}^1\pi\pi^*$ excitation energies. In addition, the ${}^1\pi\sigma^*$ state possesses considerable Rydberg character at the ground-state equilibrium geometry and its energy is therefore highly sensitive to the inclusion of diffuse functions in the basis set. However, the vertical excitation energy of the ${}^1\pi\sigma^*$ state is less relevant than the energy of the barrier for dissociation of the NH bond. In the vicinity of the barrier, the σ^* orbital contracts from a 3s-type Rydberg orbital toward the 1s orbital of the hydrogen atom.²⁶ The energy of this saddle point is therefore less basis-set dependent than the vertical excitation energy of the ${}^1\pi\sigma^*$ state.

The canonical Hartree–Fock (HF) molecular orbitals (MOs) of indole at the equilibrium geometry of the electronic ground state are displayed in Figure 4. The two highest occupied MOs (HOMOs) are of π character and are shown in Figure 4a,b. The lowest unoccupied MO (LUMO) is of π^* character (Figure 4c).

The σ^* orbital, shown in Figure 4d, is primarily located on the NH group and is considerably more diffuse than the π and π^* orbitals, as discussed above. The canonical orbitals obtained from CASSCF calculations for the ${}^1\pi\pi^*$ and ${}^1\pi\sigma^*$ states are rather similar to the canonical HF orbitals shown in Figure 4. The qualitative character of excited-state electronic wave functions can thus be discussed in terms of ground-state HF orbitals, although the unoccupied HF orbitals have, strictly speaking, no physical meaning.

It should be noted that the charge distribution of the σ^* orbital is located to a significant extent outside the atomic frame. The $\pi \rightarrow \sigma^*$ excitation is therefore of considerable CT character and results in a significant dipole moment of the ${}^1\pi\sigma^*$ state (9.5 Debye; see SI). This CT character of the ${}^1\pi\sigma^*$ state and the antibonding nodal character of the σ^* orbital provide the driving force for the ejection of the hydrogen atom and thus dissociation to two radicals. The detachment of the proton, on the other hand, would lead to an ion pair. The ion-pair formation could be driven by the ${}^1\pi\pi^*$ excited states. Our calculations do not provide evidence of a tendency of ion-pair dissociation of the 1L_b and 1L_a states (see Figure 3). There is ample computational as well as experimental evidence that the threshold for excited-state H-atom detachment (biradical dissociation) is lower than the threshold for excited-state deprotonation (ion-pair dissociation) in pyrrole, indole, and phenol.^{24–26,30–40}

Alternatively to dissociation, the departing hydrogen atom can bind at other positions of the indolyl radical, resulting in the formation of a tautomeric species. The energies and spectroscopic data of two such tautomers are given in the SI (indole–iso(C₂H₂), indole–iso(C₇H₂)), where the departing hydrogen atom is attached to the carbon atom of the ring at the positions 2 and 7, respectively). These tautomers are photochromic species, because they absorb at longer wavelengths than indole. Although they are significantly higher in energy, they are presumably rather long-lived species, because the barriers for rearrangement to indole are quite high (>1 eV⁴¹).

4. Photoinduced Hydrogen Transfer from Aromatic Chromophores to Solvent Molecules: The Indole–Ammonia Complex

Indole is the chromophore of the amino acid tryptophan. It is well-known that the fluorescence properties of tryptophan are highly sensitive to the environment.^{42,43} This unique property of tryptophan is widely used for the investigation of the structure and dynamics of proteins.^{44,45} An important photochemical channel of tryptophan in aqueous solution is photoionization, that is, the formation of hydrated electrons.⁴⁶

Indole–water or indole–ammonia clusters are good model systems for the investigation of the photoinduced elementary processes occurring in solutions of indole or tryptophan in hydrogen-bonding solvents. The excited-state dynamics of indole–solvent clusters has extensively been investigated for more than 20 years; see refs 47–52 and the references therein. In the early investigations, the possible inversion of the energetic order of the L_b and L_a states with increasing cluster size and the possible effects of L_b – L_a mixing have been the topic of interest.^{47–49} In 2001, Jouvet and co-workers discovered the importance of the hydrogen-transfer process from the photoexcited indole to ammonia, resulting in long-lived NH₄(NH₃)_n clusters.⁵⁰ The dynamics of the ultrafast hydrogen transfer and the ensuing cluster fragmentation processes have been investigated with femtosecond time-resolved spectroscopy by Hertel, Radloff, and collaborators.^{51–53}

The calculated PE profiles for the excited-state hydrogen-transfer reaction in the indole–ammonia cluster are shown in

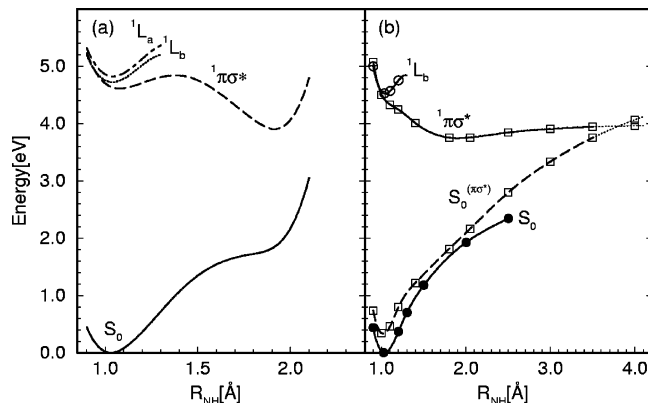


Figure 5. Potential-energy profiles of the ground state and the lowest excited states of the indole–ammonia complex as a function of the proton-transfer ($N_{ln}H$ stretching) coordinate: (a) rigid dissociation; (b) energy profiles along the minimum-energy path in the ground state and in the excited states (solid lines). The dashed line in (b) represents the energy of the ground state calculated at the geometry of the ${}^1\pi\sigma^*$ state (designated as $S_0({}^1\pi\sigma^*)$). Dotted lines indicate interpolations through regions where the CC2 calculations cannot be converged or are not considered to be reliable.

Figure 5. As before, the left-hand panel (a) shows the PE functions for rigid H-transfer (i.e., all other intramolecular and intermolecular coordinates are frozen at the ground-state equilibrium values), and the right-hand panel (b) gives the PE profiles along the minimum-energy path for hydrogen transfer. In the electronic ground state, the transfer of a proton from indole to ammonia is energetically highly unfavorable; see Figure 5. The inflection of the S_0 PE function in Figure 5a reflects the incipient ion-pair formation. The presence of ammonia lowers the excitation energy of the highly polar ${}^1\pi\sigma^*$ state; it becomes the lowest vertically excited-state at the CC2/aug-cc-pVDZ level, whereas the 1L_a state remains above the 1L_b state (see Figure 5a). It is seen that the transfer of a hydrogen atom from indole to ammonia is energetically favorable in the ${}^1\pi\sigma^*$ state. Although the PE profile for rigid H-transfer exhibits a barrier (Figure 5a), the energy profile along the minimum-energy path is barrierless (Figure 5b). The coordinate that is primarily responsible for the elimination of the barrier is the contraction of the distance between the hydrogen-bonded molecular units. The minimum of the ${}^1\pi\sigma^*$ PE function in Figure 5b at a NH distance of about 1.9 Å corresponds to the indolyl–NH₄ biradical. The fragmentation of the latter can lead to the formation of the free NH₄ radical.^{50,51} Because the S_0 PE profile of the indole–ammonia complex is flatter than for bare indole, the intersection between the ${}^1\pi\sigma^*$ and S_0 energy surfaces is shifted to significantly larger NH distances; cf. Figures 3b and 5b. Ritz et al. have calculated a two-dimensional PE surface, considering both the NH and the NN distances.⁵⁴

The MOs involved in the $\pi \rightarrow \sigma^*$ excitation at the ground-state equilibrium geometry are displayed in Figure 6. While the π orbital is compact and delocalized over the indole ring, the σ^* orbital is diffuse and mostly localized on the ammonia molecule. The $\pi \rightarrow \sigma^*$ vertical excitation thus corresponds to the transfer of electronic charge from the indole ring to a spatial region which is beyond the solvent molecule (see Figure 6b). Upon geometry optimization, the proton of the azine group of indole follows the electron, resulting in the formation of the indolyl–ammonium biradical. The two radicals are connected by a relatively strong hydrogen bond ($R_{NH} = 1.869$ Å).

It should be kept in mind that the 1L_b and ${}^1\pi\sigma^*$ PE profiles in Figure 5b correspond to different geometries. The crossing of the 1L_b and ${}^1\pi\sigma^*$ energy functions near the minimum of the

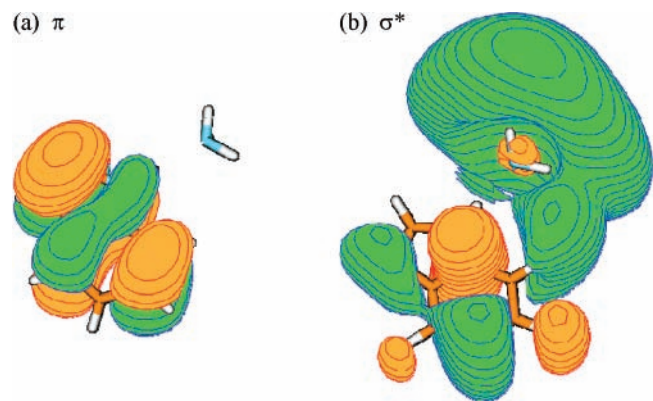


Figure 6. π (a) and the σ^* (b) Hartree–Fock molecular orbitals of the ${}^1\pi\sigma^*$ state of the indole–ammonia complex determined at the equilibrium geometry of the electronic ground state.

1L_b state is therefore an apparent crossing. The two reaction paths (in the 1L_b and ${}^1\pi\sigma^*$ states, respectively) are separated by a barrier; see also ref 54.

Though we have focused the discussion on indole–ammonia clusters in supersonic jets, the results of Figure 6 (and analogous results for indole–water clusters) are also of relevance for the rationalization of the photochemistry of indole in protic solvents.^{46,55,56} The photoinduced ejection of hydrogen atoms in water, yielding H₃O radicals, can explain the observed formation of solvated electrons with photon energies as low as 4.0 eV,⁴⁶ much below the presumed ionization potential of indole in water. It has been shown that the H₃O radical undergoes a spontaneous charge-separation process in an aqueous environment, yielding a hydrated hydronium ion and a hydrated electron.^{57,58}

5. Photoinduced Hydrogen Transfer from Solvent Molecules to Aromatic Chromophores: The Pyridine–Ammonia Complex

In this section, we consider an aromatic chromophore (pyridine) that acts as a proton acceptor in the hydrogen bonding with ammonia or water. It seems that such complexes have less extensively been investigated by spectroscopy in supersonic jets than complexes of aromatic proton donors with water or ammonia. We are not aware of experimental data on the pyridine–ammonia cluster. The vibrational spectroscopy of the pyridine–water complex has been investigated in rare-gas matrices and in the liquid phase, as well as with DFT and MP2 calculations.^{59–61}

The calculations predict a pyridine–ammonia hydrogen-bond length of 2.22 Å in the electronic ground state and 2.25 Å in the ${}^1\pi\pi^*$ excited state. The hydrogen bond is thus rather weak in both cases. In the lowest excited-state of pyridine (${}^1n\pi^*$), the hydrogen bond is even weaker (bond length 2.90 Å).

The PE functions for the rigid transfer of a hydrogen atom from ammonia to pyridine in the S_0 , ${}^1n\pi^*$, and ${}^1\pi\pi^*$ states of the pyridine–ammonia complex are shown in Figure 7a. It is seen that the H-transfer is energetically highly unfavorable in the electronic ground state. The excited-state PE functions, on the other hand, exhibit well-developed minima corresponding to the transfer of an H-atom from ammonia to pyridine; see Figure 7a. The substantial barriers separating the two minima reflect the weakness of the hydrogen bond in the ${}^1n\pi^*$ and ${}^1\pi\pi^*$ excited states. More details on the excitation energies are given in the SI.

The frontier MOs of the pyridine–ammonia complex are displayed in Figure 8. The ${}^1\pi\pi^*$ excited state (A' symmetry) is

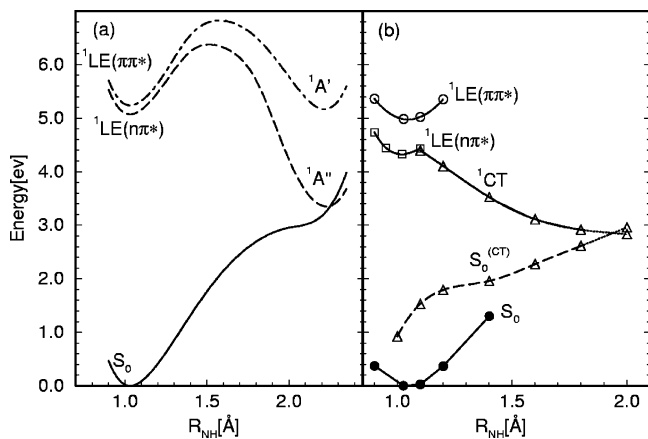


Figure 7. Potential-energy profiles of the ground state and the lowest excited singlet states of the pyridine–ammonia complex as a function of the proton-transfer ($N_{Am}H$ stretching) coordinate: (a) rigid transfer; (b) energy profiles along the minimum-energy path in the ground state and in the excited states (solid lines). The dashed line in (b) represents the energy of the ground state calculated at the geometry of the 1CT state (designated as $S_0^{(CT)}$).

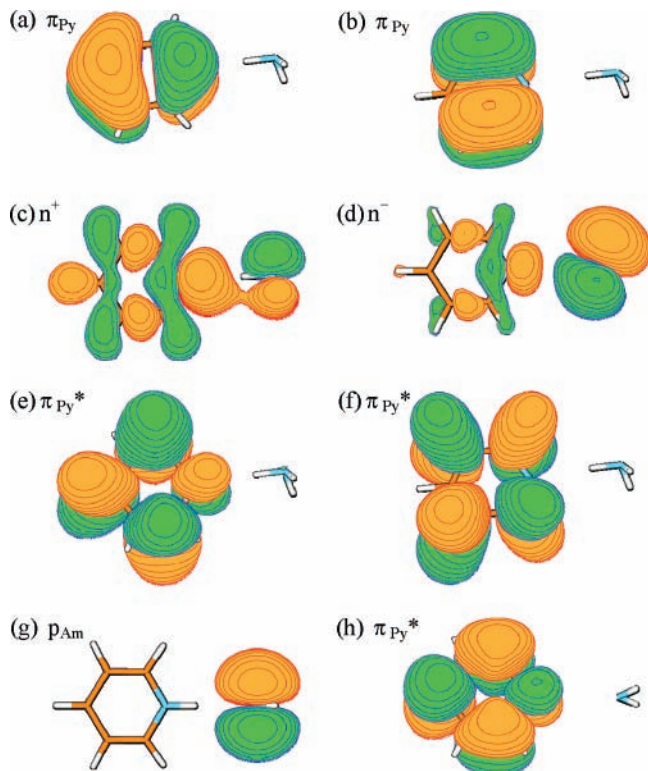


Figure 8. Two highest occupied π orbitals (a, b), the two highest occupied n orbitals (c and d), and the two lowest unoccupied π^* orbitals (e, f) of the pyridine–ammonia complex, determined at the equilibrium geometry of the electronic ground state. The singly occupied orbitals of the CT state, determined at $N_{Am}H = 1.9 \text{ \AA}$, are shown in (g) and (h).

a mixture of configurations that correspond to excitation from the two highest π orbitals (a, b) to the two lowest π^* orbitals (e, f). The ${}^1\pi\pi^*$ state clearly is a locally excited (LE) state of pyridine, but this is not the case for the lowest excited-state of A'' symmetry. This state corresponds to the excitation from n-type orbitals (c, d) to the lowest two π^* orbitals (e, f). The n-type orbitals are delocalized over both pyridine and ammonia (Figure 8c,d). Excitation from these orbitals to the π^* orbitals thus results in a certain amount of CT from ammonia to pyridine. This CT character explains the pronounced stabilization of the

${}^1n\pi^*$ state by the transfer of a proton from ammonia to pyridine. The concomitant destabilization of the ground state results in a conical intersection near the minimum of the A'' state, which corresponds to the $\text{PyH}\cdots\text{NH}_2^*$ biradical (see Figure 7a).

The optimization of the geometry of the biradical results in a structure of C_{2v} symmetry with coplanar NH_2^* and PyH^* radicals. The singly occupied MOs of this biradical are shown in Figure 8g,h. It is seen that the unpaired electrons occupy a p orbital on the NH_2 fragment as well as a π^* orbital on the PyH fragment. The PE profiles along the minimum-energy path for hydrogen transfer from ammonia to pyridine are given in Figure 7b. Note the remarkable difference between the PE profiles for rigid H-transfer and H-transfer along the minimum-energy path. Upon stretching of the NH bond of ammonia, the LE excited state of ${}^1n\pi^*$ character is crossed by a singlet CT state of $p_{Am}\pi^*_{Py}$ character, which in turn crosses the electronic ground state near $R_{NH} = 2.0 \text{ \AA}$ (see Figure 7b). The CT state connects the ${}^1\text{LE}(n\pi^*)$ state with the electronic ground state in an essentially barrierless manner. Assuming fast ${}^1\pi\pi^*\rightarrow{}^1n\pi^*$ internal conversion after excitation of the strongly allowed ${}^1\pi\pi^*$ state (as is typical for pyridine⁶²), we expect ultrafast deactivation of the complex via the transfer (in ${}^1\text{CT}$) and back-transfer (in S_0) of a hydrogen atom. We thus predict efficient quenching of the fluorescence of pyridine by complexation with ammonia. We are not aware of an experimental observation of this phenomenon.

In contrast to the ${}^1\pi\sigma^*$ mediated hydrogen-detachment (section 3) and hydrogen-transfer (section 4) processes, the pyridine–ammonia H-transfer photochemistry involves only compact valence-type frontier orbitals; see Figure 8. The reason is that the proton-accepting pyridine is, other than ammonia or water, an unsaturated system that allows the transfer of an electron into valence-type unoccupied orbitals.

6. Photoinduced Hydrogen Transfer between Hydrogen-Bonded Aromatic Chromophores: The Indole–Pyridine Complex

The phenomenon of fluorescence quenching through intermolecular hydrogen bonding between aromatic systems is a well-known phenomenon. In numerous studies, Förster, Weller, Mataga, Waluk, and co-workers have investigated the photophysics of aromatic hydrogen donor–acceptor pairs in various solvents.^{9–14,63–68} Mataga has advocated a generic model of fluorescence quenching emphasizing the role of CT states that drive proton transfer from the hydrogen donor to the hydrogen acceptor. Curve crossings of the CT state with LE states facilitate rapid internal conversion.^{12,13} The motivation for this model has been provided by an early qualitative MO-configuration-interaction calculation of Tanaka and Nishimoto, who had calculated PE profiles for (rigid) excited-state H-transfer in phenol–pyridine and aniline–pyridine complexes.⁶⁹

We adopt here the indole–pyridine hydrogen-bonded complex for the investigation of excited-state electron and proton-transfer processes in hydrogen-bonded aromatic pairs. Two conformers of the indole–pyridine complex were obtained by geometry optimization with C_s symmetry constraint at the MP2/cc-pVDZ level. The two conformers correspond to a parallel and perpendicular arrangement of the aromatic rings, respectively. Both conformers exhibit a fairly strong hydrogen bond (bond length 1.95 Å). The perpendicular conformer is more stable than the planar conformer by about 1 kcal/mol (see SI). The lowest excited singlet states of both conformers result from excitations within the indole ring (1L_b , ${}^1\pi\sigma^*$, 1L_a ; see SI).

We choose the planar conformer for further investigations, because this conformer is more representative for the photo-

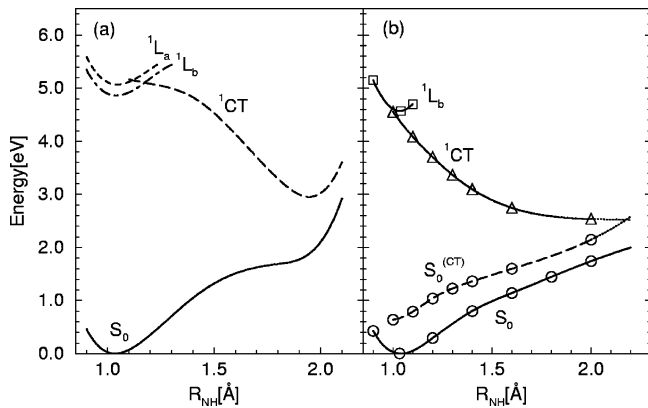


Figure 9. Potential-energy profiles of the ground state and the lowest excited singlet states of the indole–pyridine complex as a function of the proton-transfer ($N_{in}H$ stretching) coordinate: (a) rigid transfer; (b) energy profile along the minimum-energy path in the ground state and in the excited states (solid lines). The dashed line in (b) represents the energy of the ground state calculated at the geometry of the 1CT state (designated as $S_0^{(CT)}$).

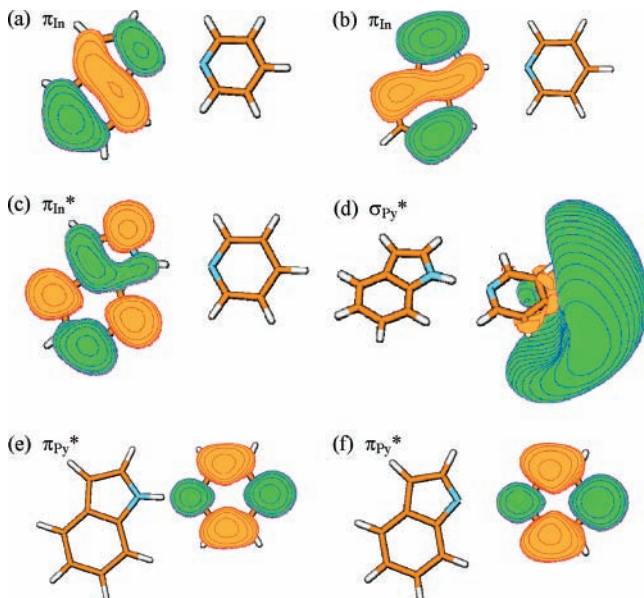


Figure 10. Two highest occupied π_{in} orbitals (a, b), the lowest unoccupied π_{in}^* orbital (c), and the σ_{Py}^* orbital (d) of the indole–pyridine complex, determined at the equilibrium geometry of the electronic ground state. The singly occupied π_{Py}^* orbital of the CT state, determined at $N_{in}H = 1.0 \text{ \AA}$ and $N_{in}H = 2.0 \text{ \AA}$, is shown in (e) and (f), respectively.

chemistry of multiply hydrogen-bonded pairs such as DNA base pairs. The PE profiles for rigid and minimum-energy H-transfer from indole to pyridine are shown in Figure 9. The frontier orbitals of this complex are displayed in Figure 10. It is seen from Figure 9a that both LE states of indole are crossed by a CT state not far from their minima. For the planar complex, the CT state is of the same symmetry species (A') as the LE states of indole. Its wave function is dominated by electronic excitations from the π orbitals of indole (see Figure 10a,b) to the lowest π^* orbital of pyridine (Figure 10e). The latter is insensitive to the location of the proton; see Figure 10e (proton attached to indole) and Figure 10f (proton attached to pyridine). It is noteworthy that the PE energy profile of the CT state is barrierless even for rigid transfer of the proton (Figure 9a). The $^1\pi\sigma^*$ state of indole is higher in energy and does not play a role for the dynamics of the lowest excited states of the indole–pyridine complex.

The PE profiles along the minimum-energy path for hydrogen transfer are shown in Figure 9b. The geometry-optimized CT energy crosses both the 1L_b PE function (near its minimum) and the PE profile of the electronic ground state. As discussed above for other systems, the 1L_b – 1CT crossing is an apparent crossing, while the 1CT – $S_0^{(CT)}$ crossing is a true crossing (conical intersection). Because the 1CT – S_0 conical intersection can be reached directly via a strongly repulsive PE function, we expect a very rapid depopulation of the 1CT state. The transition from the 1L_b state to the 1CT state, which may involve a barrier, should be the rate-limiting step in the deactivation of the 1L_b state. This conclusion is in agreement with femtosecond/picosecond time-resolved spectroscopic data of Mataga and co-workers for pyrenol–pyridine and related systems.^{65–67} Figure 9b fully confirms the qualitative model of fluorescence quenching proposed by Mataga, in particular the role of the 1CT state which connects the $LE(^1\pi\pi^*)$ state with the S_0 state via two conical intersections.^{12,13}

The same mechanism has recently been investigated for multiply hydrogen-bonded aromatic pairs, such as the 2-aminoypyridine (2AP) dimer as well as the guanine–cytosine (GC) and adenine–thymine (AT) DNA base pairs.^{70–73} Femtosecond time-resolved pump–probe measurements have revealed that the excited-state lifetime is shortened by a factor of 20 in the hydrogen-bonded dimer of 2AP compared to the monomer.⁷⁴ The enhanced excited-state deactivation through hydrogen bonding has been confirmed for the Watson–Crick structure of the GC dimer both in the gas phase and in solution.^{75,76}

7. Photoinduced Intramolecular Hydrogen Transfer in Bifunctional Aromatic Systems: 7-(2'-Pyridyl)indole

Pyridylindoles and pyridylpyrroles are bifunctional aromatic chromophores possessing both a hydrogen donor and a hydrogen acceptor group. Their spectroscopy and photophysics have been studied extensively both in supersonic jets and in nonpolar and protic solvents by Waluk, Mordzinski, and collaborators.^{77–82} The 2-(2'-pyridyl)indoles cannot form strong intramolecular hydrogen bonds, but are good model systems for the investigation of fluorescence quenching via solvent wires in hydrogen-bonding solvents.^{77,79,80} 7-(2'-pyridyl)indole (7PyIn), on the other hand, possesses an intramolecular hydrogen bond in the syn configuration, which stabilizes this conformer significantly relative to the anti configuration.⁸¹ It has been shown that 7PyIn is essentially nonfluorescent in nonpolar solvents. The excited-state lifetime was found to be too short to be detected with subnanosecond time resolution.⁸¹

The ground-state equilibrium structure of the syn form of 7PyIn is shown in Figure 11a. It exhibits a moderately strong hydrogen bond (bond length 2.062 Å) between the azine group of indole and the nitrogen atom of the pyridine ring. The two rings are almost coplanar, but the PE function is very flat with respect to twisting around the CC single bond connecting the two rings. This flatness reflects the competing effects of N–H···N hydrogen bonding and steric repulsion of CH groups. The anti conformer, shown in Figure 11b, is more nonplanar (twist angle 142°) due to the absence of an intramolecular hydrogen bond. At the CC2/cc-pVDZ level, the anti form is located 0.24 eV (5.5 kcal/mol) above the syn form.

The hydrogen-transferred syn form (with the hydrogen atom attached to the pyridine ring) does not represent a minimum of the S_0 PE surface at the MP2/cc-pVDZ level. The anti configuration of this tautomer, shown in Figure 11c, is another local minimum of the S_0 surface. The twist angle of this structure is 163°, and the energy is 1.45 eV (33.4 kcal/mol) above the

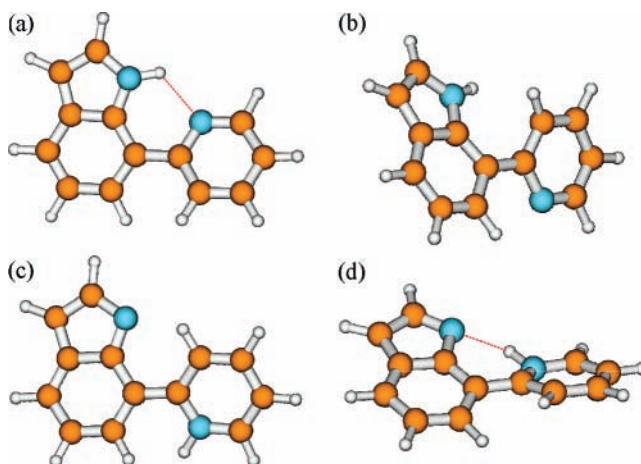


Figure 11. Ground-state equilibrium geometries of the syn (a) and anti (b) forms of 7-(2'-pyridyl)indole. The ground-state equilibrium geometry of the hydrogen-transferred structure of the anti conformer is shown in (c). The structure in (d) represents the minimum-energy structure of the hydrogen-transferred syn conformer in the S_1 state.

global S_0 minimum (at the CC2/cc-pVDZ level). Although the syn (Figure 11a) and anti (Figure 11b) conformers are separated by a low barrier of about 1 kcal/mol, the hydrogen-transferred anti conformer (Figure 11c) is separated by a barrier of 10.0 kcal/mol from the lower-energy structure.

The vertical excitation energies and oscillator strengths of the ground-state isomers of 7PyIn are given in the SI. The syn form absorbs strongly ($f = 0.32$) in the UV ($\Delta E_{\text{vert}} = 4.0$ eV). The vertical excitation energy of the $^1\pi\pi^*$ state of the anti form is 4.4 eV, slightly to the blue of the syn form. The hydrogen-transferred anti form is a photochromic species, because it has a strongly red-shifted absorption spectrum ($\Delta E_{\text{vert}} = 1.9$ eV, $f = 0.10$).

Optimization of the geometry of the $S_1(\pi\pi^*)$ state with C_s symmetry constraint, starting from the ground-state equilibrium geometry of the syn conformer, results in the barrierless transfer of a hydrogen atom to the pyridine ring. This hydrogen-transferred structure represents, however, a saddle point on the S_1 PE surface. This structure is unstable with respect to torsion around the central CC bond. The unconstrained optimization of the S_1 energy leads to a minimum-energy structure with an indole–pyridine twist angle of 33° and a slightly pyramidal N atom of the pyridine ring (the sum of the bond angles is 355°). The energy of this S_1 minimum lies 2.8 eV above the global minimum of the S_0 surface. At this S_1 minimum-energy geometry, the ground-state energy lies only 1.2 eV below the S_1 energy (CC2/cc-pVDZ values).

Figure 12 provides an overview of the PEs of 7PyIn as functions of the hydrogen-transfer coordinate (NH bond length) and the inter-ring twisting coordinate (CCCN dihedral angle) in the S_0 and S_1 states. These minimum-energy-path profiles were obtained by calculating the CC2/cc-pVDZ energy of the S_0 and S_1 states at geometries that were optimized at the MP2/SV(P) and CC2/SV(P) levels, respectively. In addition, the energy profiles of the ground state calculated at the optimized geometry of the excited state, $S_0^{(S_1)}$, are shown (dashed lines).

Figure 12a shows the PE functions for torsion of 7PyIn. The global ground-state minimum (syn form, Figure 11a) is nearly planar. The anti form (Figure 11b) shows up as a shallow minimum near 140°, separated by a low barrier of about 1 kcal/mol. The torsional barrier is more pronounced in the S_1 state. For dihedral angles $\theta(\text{CCCN})$ below 60°, spontaneous hydrogen

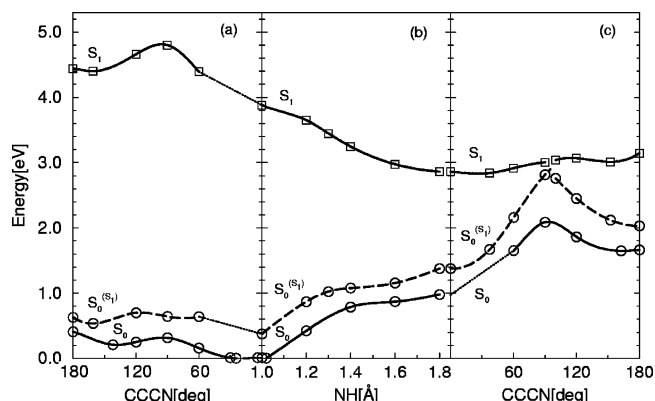


Figure 12. Potential-energy energy profiles of the S_0 state (circles) and the $S_1(\pi\pi^*)$ state (squares) of 7-(2'-pyridyl)indole as a function of the torsional reaction path (a, c) and the hydrogen-transfer reaction path (b). Full lines: energy profiles of reaction paths determined in the same electronic state. The dashed lines represent the energy of the ground state calculated at the geometry of the S_1 state (designated as $S_0^{(S_1)}$). The dotted lines in (a) and (c) denote interpolations where reaction-path optimizations were not possible.

transfer takes place, resulting in the H-transferred syn conformer of 7PyIn (Figure 11d). This part of the PE function is represented by the dotted line in Figure 12a.

The energy profiles for the hydrogen-transfer reaction of the syn conformer of 7PyIn are displayed in Figure 12b. As is typical for ESIPT systems, the hydrogen-transfer process is endothermic in the electronic ground state, but exothermic in the S_1 state. In both cases, the minimum-energy-path potential function is barrierless. As mentioned above, the hydrogen-transferred S_1 surface is unstable with respect to torsion around the central CC bond.

The torsional PE profiles for the hydrogen-transferred tautomer of 7PyIn are shown in Figure 12c. The minimum-energy profile of the S_0 state clearly exhibits a minimum near 180°, which corresponds to the structure of Figure 11c. Like in Figure 12a, spontaneous hydrogen transfer takes place for dihedral angles $\theta(\text{CCCN})$ below 60°, resulting in the normal syn conformer of 7PyIn (Figure 11a). This part of the PE function is represented by the dotted line in Figure 12c. The minimum-energy path in the S_1 state could be followed from $\theta = 0^\circ$ (planar system) through the minimum of the S_1 state ($\theta = 33^\circ$) up to $\theta = 90^\circ$. At this geometry, the $S_1 - S_0$ energy gap vanishes. The same result was obtained when the minimum-energy path in S_1 was followed from $\theta = 180^\circ$ down to $\theta = 90^\circ$. Although the CC2 method, being a single-reference method, is stretched to the limit by these calculations, the results of Figure 12c provide strong evidence for the existence of a conical intersection between the S_1 and S_0 surface at a dihedral angle near 90°. A more accurate characterization of this conical intersection requires the use of MCSCF and MRCI methods.

To provide insight into the electronic structure of the states involved in the photophysics of 7PyIn, we display in Figure 13 the HOMO (π_H) and LUMO (π_L^*), which are singly occupied in the S_1 state, at the planar S_0 equilibrium geometry (a, b), the hydrogen-transferred S_1 state (c, d) and at the perpendicular geometry ($\theta = 90^\circ$) close to expected $S_1 - S_0$ conical intersection (e, f). Only the π_H/π_L^* orbitals of the aromatic rings are involved as frontier orbitals. It can be seen that the $S_0 \rightarrow S_1$ excitation at the S_0 equilibrium geometry is accompanied by a small shift of electron density from the indole ring to the pyridine ring. At the S_1 minimum, the ground state is highly polar ($\mu = 8.2$ Debye) due to the nearly complete localization of the HOMO on the indole ring (Figure 13c), whereas the proton has been

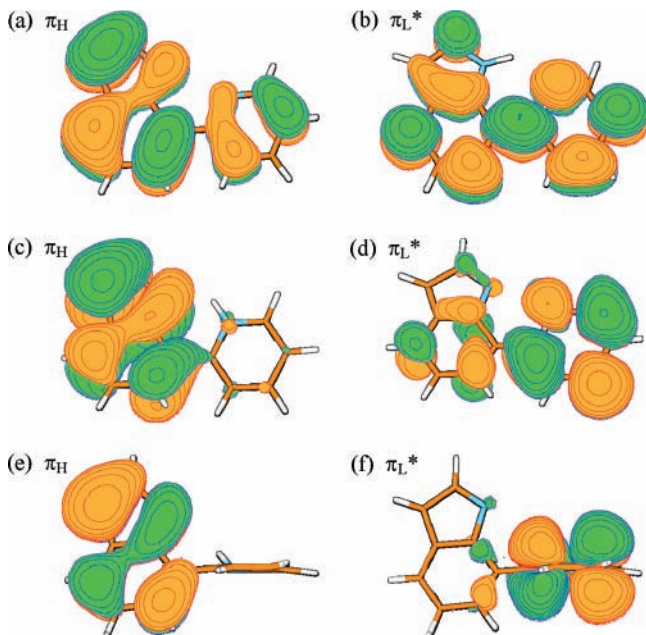


Figure 13. Highest occupied orbital (π_H) and the lowest unoccupied orbital (π_{L^*}) of 7-(2'-pyridyl)indole, determined at (a, b) the equilibrium geometry of the electronic ground state, (c, d) the equilibrium geometry of the S_1 state, and (e, f) near the S_1-S_0 intersection ($\theta(\text{CCCN}) = 90^\circ$).

transferred to the pyridine ring. This polarity is strongly reduced in the S_1 state ($\mu = 4.2$ Debye) due to the delocalized character of the LUMO (Figure 13d). At the geometry close to the S_1-S_0 conical intersection, the HOMO and LUMO are completely localized on indole and pyridine, respectively (Figures 13e,f). 7PyIn at this configuration thus is an almost perfect biradical, as is typical for a degeneracy of the open-shell S_1 state with the closed-shell ground state.⁸³

In intermolecularly hydrogen-bonded aromatic systems the hydrogen-transfer process leads directly to a conical intersection with the electronic ground state (cf. Figure 9b), but this is not the case in intramolecularly hydrogen-bonded π systems; see Figure 12b. A very similar picture as in Figure 12 has also been found for the ESIPT systems salicylic acid, methylsalicylate, and 2-(2'-hydroxyphenyl)benzotriazole (TINUVIN).^{84–86} It seems thus generic that intramolecularly hydrogen-bonded aromatic systems require a torsional motion to reach the conical intersection of the S_1 and S_0 surfaces, where the radiationless deactivation takes place. On the other hand, in the intramolecularly hydrogen-bonded aromatic systems optical excitation leads directly to the PT-reactive state and, unlike in the intermolecularly hydrogen-bonded systems, the nonadiabatic LE-CT transition is not involved in the PT process.

8. Conclusions

We have discussed in this Feature Article generic mechanisms of excited-state deactivation via hydrogen-atom dynamics in isolated aromatic chromophores, their complexes with amphoteric solvent molecules, hydrogen-bonded pairs of aromatic chromophores, and bifunctional intramolecularly hydrogen-bonded aromatic systems. It has been shown that excited-state reactions involving the detachment or transfer of a hydrogen atom play a decisive role for the photophysics of all these systems. While photoinduced hydrogen detachment from acidic chromophores and hydrogen transfer to saturated solvent molecules are driven by ${}^1\pi\sigma^*$ states with pronounced Rydberg character, the hydrogen-transfer processes from saturated solvent

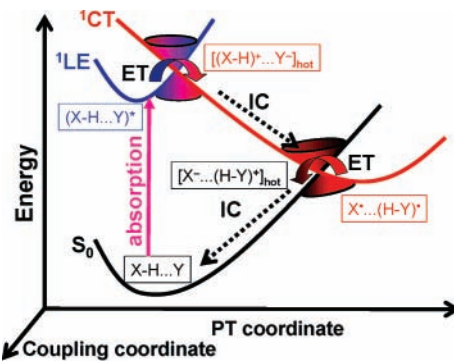


Figure 14. Schematic view of the EDPT process in intermolecularly hydrogen-bonded systems. Abbreviations: LE, locally excited state; CT, charge-transfer state; ET, electron transfer; IC, internal conversion. The colors indicate schematically the mixing of the electronic wave functions at the conical intersections.

molecules to basic π chromophores as well as between π systems are driven by compact valence-type CT states. In all examples considered here, conical intersections of the S_1 and S_0 PE surfaces, which become accessible via the detachment or transfer of a hydrogen atom, play a crucial role in the ultrafast photophysics.

The common motif of the various photochemical reaction mechanisms is the electron-driven proton-transfer (EDPT) process. The hydrogen detachment via ${}^1\pi\sigma^*$ states is at least partially driven by the high polarity of these states, arising from the localization of the σ^* electron density outside the aromatic ring. Hydrogen transfer in acidic chromophore-solvent clusters is driven by the localization of the σ^* charge density on the solvent molecule. Once the ${}^1\pi\sigma^*$ state is populated (usually by curve crossing from the allowed ${}^1\pi\pi^*$ states), the proton follows the electron, leading to a pronounced energetic stabilization of the biradical. In hydrogen-bonded aromatic pairs, it is a highly polar CT state of ${}^1\pi\pi^*$ valence character which provides the driving force for the transfer of the proton: again the proton follows the electron, resulting in a biradical structure. After the back-transfer of the electron at the S_1-S_0 conical intersection, the proton is driven back to the original location, thereby closing the photophysical cycle. This generic picture of the EDPT process is illustrated in Figure 14.

The unusually large energy gradients and the small mass of the proton ensure the exceptionally fast rate of these processes. The energy of the UV photon is converted into vibrational energy of the hydrogen bond, which subsequently is dissipated to other intramolecular as well as intermolecular vibrational degrees of freedom. The photoexcited hydrogen-bonded system thus returns to the closed-shell electronic ground state before competing photochemical reactions can take place (see Figure 14).

In planar intramolecularly hydrogen-bonded π systems, the excited-state hydrogen transfer itself does not lead to a S_1-S_0 conical intersection. However, there is now compelling evidence from the computational investigation of several characteristic ESIPT systems that the hydrogen-transfer process triggers out-of-plane torsion on the S_1 surface, which leads in a barrierless manner to a S_1-S_0 conical intersection and thus ultrafast internal conversion.^{84–86} The EDPT process illustrated in Figure 14 thus emerges as a unifying concept behind such seemingly different phenomena as H-detachment from aromatic chromophores in the gas phase, formation of solvated electrons in solution, fluorescence quenching by hydrogen bonding, the function of commercial organic photostabilizers, and the photostability of biological molecules such as DNA and proteins.⁸⁷

In this Feature Article, we have emphasized qualitative concepts for the rationalization of photochemical dynamics, such as minimum-energy reaction paths, PE profiles, and properties of frontier orbitals. More quantitative theoretical studies have to address the treatment of the nuclear dynamics, including barrier tunneling, the dynamics at conical intersections, and intramolecular vibrational relaxation (IVR). The first steps in this direction have been done, employing either quantum wave packet dynamics for reduced-dimensional ab initio models (see, e.g., refs 30 and 31) or full-dimensional on-the-fly trajectory or Gaussian wave packet calculations (see, e.g., refs 88–91). It can be envisioned that the combined efforts of ab initio computational studies and advanced spectroscopic experiments will lead to a new level of understanding of organic photochemistry and photobiology.

Acknowledgment. This work has been supported by a joint research grant of the Deutsche Forschungsgemeinschaft (DFG) and the Ministry of Science and Education of Poland. A.L.S. acknowledges partial support by a visitor grant of the DFG Cluster of Excellence “Munich Centre of Advanced Photonics” (www.munich-photonics.de).

Supporting Information Available: Tables of spectroscopic properties: energy of vertical absorption ($\Delta E/\text{eV}$), oscillator strength (f), and dipole moment (μ/Debye) of molecular systems pertaining to this work, calculated with the CC2 method at the MP2 ground-state equilibrium geometry. This material is available free of charge via the Internet at <http://pubs.acs.org>.

References and Notes

- (1) Pimentel, G. C.; McClellan, A. L. *The Hydrogen Bond*; Freeman, San Francisco, 1960.
- (2) Iftimie, R.; Minary, P.; Tuckerman, M. E. *Proc. Natl. Acad. Sci. U.S.A.* **2005**, *102*, 6654.
- (3) Marx, D. *ChemPhysChem* **2006**, *7*, 1848.
- (4) Formosinho, S. J.; Arnaut, L. G. *J. Photochem. Photobiol. A* **1993**, *75*, 21.
- (5) Ormson, S. M.; Brown, R. G. *Prog. React. Kinet.* **1994**, *19*, 45. Le Gourrierec, D.; Ormson, S. M.; Brown, R. G. *Prog. React. Kinet.* **1994**, *19*, 211.
- (6) Douhal, A.; Lahmani, F.; Zewail, A. H. *Chem. Phys.* **1996**, *207*, 477.
- (7) Heller, H. J.; Blattmann, H. R. *Pure Appl. Chem.* **1972**, *30*, 145; **1974**, *36*, 141.
- (8) Otterstedt, J.-E. A. *J. Chem. Phys.* **1973**, *58*, 5716.
- (9) Förster, T. Z. *Elektrochem.* **1950**, *54*, 531.
- (10) Rehm, D.; Weller, A. *Isr. J. Chem.* **1970**, *8*, 259.
- (11) Arnaut, L. G.; Formosinho, S. J. *J. Photochem. Photobiol. A* **1993**, *75*, 1.
- (12) Mataga, N. *Pure Appl. Chem.* **1984**, *56*, 1255.
- (13) Mataga, N. *Adv. Chem. Phys.* **1999**, *107*, 431.
- (14) Waluk, J. *Acc. Chem. Res.* **2003**, *36*, 832.
- (15) Rini, M.; Magnes, B.-Z.; Pines, E.; Nibbering, E. T. *J. Science* **2003**, *301*, 349.
- (16) Mohammed, O. F.; Pines, D.; Dreyer, J.; Pines, E.; Nibbering, E. T. *J. Science* **2005**, *310*, 83.
- (17) *Modern Electronic Structure Theory*; Yarkony, D. R., Ed. World Scientific: Singapore, 1995; Parts I and II.
- (18) Christiansen, O.; Koch, H.; Jørgensen, P. *Chem. Phys. Lett.* **1995**, *243*, 409.
- (19) Hättig, C.; Weigend, F. *J. Chem. Phys.* **2000**, *113*, 5154.
- (20) Köhn, A.; Hättig, C. *J. Chem. Phys.* **2003**, *119*, 5021.
- (21) Woon, D. E.; Dunning, T. H., Jr. *J. Chem. Phys.* **1993**, *98*, 1358.
- (22) Ahlrichs, R.; Bär, M.; Häser, M.; Horn, H.; Kölmel, C. *Chem. Phys. Lett.* **1989**, *162*, 165.
- (23) Weigend, F.; Häser, M. *Theor. Chem. Acc.* **1997**, *97*, 331.
- (24) Sobolewski, A. L.; Domcke, W. *Chem. Phys. Lett.* **1999**, *315*, 293.
- (25) Sobolewski, A. L.; Domcke, W. *Chem. Phys.* **2000**, *259*, 181.
- (26) Sobolewski, A. L.; Domcke, W.; Dedonder-Lardeux, C.; Jouvet, C. *Phys. Chem. Chem. Phys.* **2002**, *4*, 1093.
- (27) Robb, M. A.; Bernardi, F.; Olivucci, M. *Pure Appl. Chem.* **1995**, *67*, 783.
- (28) Yarkony, D. R. *Rev. Mod. Phys.* **1996**, *68*, 985.
- (29) *Conical Intersections: Electronic Structure, Dynamics and Spectroscopy*; Domcke, W., Yarkony, D. R., Köppel, H., Eds.; World Scientific: Singapore, 2004.
- (30) Lan, Z.; Domcke, W.; Vallet, V.; Sobolewski, A. L.; Mahapatra, S. *J. Chem. Phys.* **2005**, *122*, 224315.
- (31) Vallet, V.; Lan, Z.; Mahapatra, S.; Sobolewski, A. L.; Domcke, W. *J. Chem. Phys.* **2005**, *123*, 144307.
- (32) Blank, D. A.; North, S. W.; Lee, Y. T. *Chem. Phys.* **1994**, *187*, 35.
- (33) Wei, J.; Kuczmann, A.; Renth, F.; Temps, F. *Phys. Chem. Chem. Phys.* **2003**, *5*, 315.
- (34) Cronin, B.; Nix, M. G. D.; Qadiri, R. H.; Ashfold, M. N. R. *Phys. Chem. Chem. Phys.* **2004**, *6*, 5031.
- (35) Lippert, H.; Ritze, H. H.; Hertel, I. V.; Radloff, W. *ChemPhysChem* **2004**, *5*, 1423.
- (36) Tseng, C. M.; Lee, Y. T.; Ni, C. K. *J. Chem. Phys.* **2004**, *121*, 2459.
- (37) Ashfold, M. D. R.; Cronin, B.; Devine, A. L.; Dixon, R. N.; Nix, M. G. D. *Science* **2006**, *312*, 1637.
- (38) Lan, Z.; Dupays, A.; Vallet, V.; Mahapatra, S.; Domcke, W. *J. Photochem. Photobiol. A* **2007**, *190*, 177.
- (39) Lin, M. F.; Tseng, C.-M.; Lee, Y. T.; Ni, C.-K. *J. Chem. Phys.* **2005**, *123*, 124303.
- (40) Nix, M. G. D.; Devine, A. L.; Cronin, B.; Ashfold, M. N. R. *Phys. Chem. Chem. Phys.* **2006**, *8*, 2610.
- (41) Sobolewski, A. L.; Domcke, W. *ChemPhysChem* **2007**, *8*, 756.
- (42) Lumry, R.; Herschberger, M. *Photochem. Photobiol.* **1978**, *27*, 819.
- (43) Szabo, A. G.; Rayner, D. M. *J. Am. Chem. Soc.* **1980**, *102*, 554.
- (44) Engelborghs, Y. *Spectrochim. Acta A* **2001**, *57*, 2255.
- (45) Marquezin, C. A.; Hirata, I. Y.; Juliano, L.; Ito, A. S. *Biopolymers* **2003**, *71*, 569.
- (46) Bent, D. V.; Hayon, E. *J. Am. Chem. Soc.* **1975**, *97*, 2612.
- (47) Hager, J. W.; Demmer, D. R.; Wallace, S. C. *J. Phys. Chem.* **1987**, *91*, 1375.
- (48) Tubergen, M. J.; Levy, D. H. *J. Phys. Chem.* **1991**, *95*, 2175.
- (49) Carney, A. J. R.; Zwier, T. S. *J. Phys. Chem.* **1999**, *103*, 9943.
- (50) Dedonder-Lardeux, C.; Grosswasser, D.; Jouvet, C.; Martrenchard, S. *PhysChemComm* **2001**, *4*, 1.
- (51) Lippert, H.; Stert, V.; Hesse, L.; Schulz, C. P.; Hertel, I. V.; Radloff, W. *J. Phys. Chem. A* **2003**, *107*, 8239.
- (52) Lippert, H.; Stert, V.; Hesse, L.; Schulz, C. P.; Hertel, I. V.; Radloff, W. *Chem. Phys. Lett.* **2003**, *376*, 40.
- (53) Lippert, H.; Stert, V.; Schulz, C. P.; Hertel, I. V.; Radloff, W. *Phys. Chem. Chem. Phys.* **2004**, *6*, 2718.
- (54) Ritze, H.-H.; Lippert, H.; Stert, V.; Radloff, W.; Hertel, I. V. *J. Chem. Phys.* **2004**, *120*, 3619.
- (55) Peon, J.; Hess, G. C.; Percourt, J.-M. L.; Yuzawa, T.; Kohler, B. *J. Phys. Chem. A* **1999**, *103*, 2460.
- (56) Sherin, P. S.; Snytnikova, O. A.; Tsentalovich, Y. P.; Sagdeev, R. Z. *J. Chem. Phys.* **2006**, *125*, 144511.
- (57) Sobolewski, A. L.; Domcke, W. *Phys. Chem. Chem. Phys.* **2002**, *4*, 4.
- (58) Sobolewski, A. L.; Domcke, W. *J. Phys. Chem. A* **2007**.
- (59) Destexhe, A.; Smets, J.; Adamowicz, L.; Maes, G. *J. Phys. Chem.* **1994**, *98*, 1506.
- (60) Dkhissi, A.; Adamowicz, L.; Maes, G. *J. Phys. Chem. A* **2000**, *104*, 2112.
- (61) Schlücker, S.; Singh, R. K.; Asthana, B. P.; Popp, J.; Kiefer, W. *J. Phys. Chem. A* **2001**, *105*, 9983.
- (62) Innes, K. K.; Ross, I. G.; Moomaw, W. R. *J. Mol. Spectrosc.* **1988**, *132*, 492.
- (63) Mataga, N.; Tsuno, S. *Bull. Chem. Soc. Jpn.* **1957**, *30*, 711.
- (64) Mataga, N. *Bull. Chem. Soc. Jpn.* **1958**, *31*, 481.
- (65) Ikeda, N.; Okada, T.; Mataga, N. *Bull. Chem. Soc. Jpn.* **1981**, *54*, 1025.
- (66) Martin, M. M.; Ikeda, N.; Okada, T.; Mataga, N. *J. Phys. Chem.* **1982**, *86*, 4148.
- (67) Miyasaka, H.; Tabata, A.; Ojima, S.; Ikeda, N.; Mataga, N. *J. Phys. Chem.* **1993**, *97*, 8222.
- (68) Herbig, J.; Kijak, M.; Zielinska, A.; Thummel, R. P.; Waluk, J. *J. Phys. Chem. A* **2002**, *106*, 2158.
- (69) Tanaka, H.; Nishimoto, K. *J. Phys. Chem.* **1984**, *88*, 1052.
- (70) Sobolewski, A. L.; Domcke, W. *Chem. Phys.* **2003**, *294*, 73.
- (71) Sobolewski, A. L.; Domcke, W. *Phys. Chem. Chem. Phys.* **2004**, *6*, 2763.
- (72) Sobolewski, A. L.; Domcke, W.; Hättig, C. *Proc. Natl. Acad. Sci. U.S.A.* **2005**, *102*, 17903.
- (73) Perun, S.; Sobolewski, A. L.; Domcke, W. *J. Phys. Chem.* **2006**, *110*, 9031.
- (74) Schultz, T.; Somoylova, E.; Radloff, W.; Hertel, I. V.; Sobolewski, A. L.; Domcke, W. *Science* **2004**, *306*, 1765.
- (75) Abo-Riziq, A.; Grace, L.; Nir, E.; Kabelac, M.; Hobza, P.; de Vries, M. S. *Proc. Natl. Acad. Sci. U.S.A.* **2005**, *102*, 20.
- (76) Schwalb, N. K.; Temps, F. *J. Am. Chem. Soc.* **2007**, *129*, 9272.

- (77) Herbich, J.; Hung, C.-Y.; Thummel, R. P.; Waluk, J. *J. Am. Chem. Soc.* **1996**, *118*, 3508.
- (78) Nosenko, Y.; Stepanenko, Y.; Wu, F.; Thummel, R. P.; Mordzinski, A. *Chem. Phys. Lett.* **1999**, *315*, 87.
- (79) Kyrychenko, A.; Herbich, J.; Wu, F.; Thummel, R. P.; Waluk, J. *J. Am. Chem. Soc.* **2000**, *122*, 2818.
- (80) Nosenko, Y.; Thummel, R. P.; Mordzinski, A. *Phys. Chem. Chem. Phys.* **2004**, *6*, 363.
- (81) Wiosna, G.; Petkova, I.; Mudadu, M. S.; Thummel, R. P.; Waluk, J. *Chem. Phys. Lett.* **2004**, *400*, 379.
- (82) Kijak, M.; Nosenko, Y.; Singh, A.; Thummel, R. P.; Waluk, J. *J. Am. Chem. Soc.* **2007**, *129*, 2738.
- (83) Klessinger, M.; Michl, J. *Excited States and Photochemistry of Organic Molecules*; VCH: Weinheim, 1995; section 4.3.
- (84) Sobolewski, A. L.; Domcke, W. *Phys. Chem. Chem. Phys.* **2006**, *8*, 3410.
- (85) Coe, J. D.; Levine, B. G.; Martinez, T. J. DOI: 10.1021/jp072027b.
- (86) Sobolewski, A. L.; Domcke, W.; Hättig, C. *J. Phys. Chem. A* **2006**, *110*, 6301.
- (87) Sobolewski, A. L.; Domcke, W. *Europhys. News* **2006**, *37*, 20.
- (88) Ben-Nun, M.; Martinez, T. J. *Adv. Chem. Phys.* **2002**, *121*, 439.
- (89) Doltsinis, N. L.; Marx, D. *J. Theor. Comput. Chem.* **2002**, *1*, 319.
- (90) Worth, G. A.; Robb, M. A. *Adv. Chem. Phys.* **2002**, *124*, 355.
- (91) Barbatti, M.; Granucci, G.; Persico, M.; Ruckenbauer, M.; Vazdar, M.; Eckert-Maksic, M.; Lischka, H. *J. Photochem. Photobiol. A* **2007**, *190*, 228.